COMPUTATIONAL RESULTS FOR FLOWS OVER 2-D RAMP AND 3-D OBSTACLE WITH AN UPWIND NAVIER-STOKES SOLVER

Ethiraj Venkatapathy
Research Scientist, Eloret Institute
NASA Ames Research Center, Moffett Field, CA.

Abstract

An implicit, finite-difference, upwind, full Navier-Stokes solver has been applied to supersonic/hypersonic flows over two-dimensional ramps and three-dimensional obstacle (Problem sets 3 and 4). Some of the computed numerical results are presented here.

Numerical Schemes

The numerical scheme used in the present study is an implicit, spatially second order accurate, upwind, LU - ADI scheme based on Roe's approximate Reimann solver with MUSCL differencing of Van Leer[1,2]. A brief outline of the numerical method is provided below.

The Navier-Stokes equations in three-dimensions and in generalized coordinates can be written as :

$$\frac{\partial \hat{Q}}{\partial t} + \frac{\partial \hat{E}}{\partial \xi} + \frac{\partial \hat{F}}{\partial \eta} + \frac{\partial \hat{G}}{\partial \zeta} = (Re^{-1})(\frac{\partial \hat{R}}{\partial \xi} + \frac{\partial \hat{S}}{\partial \eta} + \frac{\partial \hat{T}}{\partial \zeta}) \tag{1}$$

where $\hat{Q}$ represents conservation variables, $\hat{E}$, $\hat{F}$ and $\hat{G}$ are the inviscid fluxes and $\hat{R}$, $\hat{S}$, and $\hat{T}$ are the viscous fluxes. The steady-state solution of Eq. (1) is obtained by time integration in a time-asymptotic fashion. The time marching method used here is the LU-ADI method proposed in Ref.1. The LU-ADI factorization method applied to Eq. (1) is written as,

$$[T_\xi L_\xi D_\xi U_\xi T_\xi{}^{-1}]\,[T_\eta L_\eta D_\eta U_\eta T_\eta{}^{-1}]$$
$$[T_\zeta L_\zeta D_\zeta U_\zeta T_\zeta{}^{-1}]\Delta\hat{Q}^n = RHS^n \tag{2}$$

where RHS represent the discretized steady-state terms. The RHS terms appear as,

$$RHS = -\Delta t[\delta_\xi \hat{E}^{+n} + \delta_\xi \hat{E}^{-n} + \delta_\eta \hat{F}^n + \delta_\zeta \hat{G}^n -$$

$$(Re^{-1})(\bar{\delta}_\xi \hat{R}^n + \bar{\delta}_\eta \hat{S}^n + \bar{\delta}_\zeta \hat{T}^n) - D_e \hat{Q}^n] \quad (3)$$

Inviscid fluxes, for example in the ξ direction, of Eq.(1) are written following Roe's difference procedure as,

$$\hat{E}(Q_l, Q_r)_{j,k,l} =$$
$$0.5[\hat{E}(Q_l) + \hat{E}(Q_r) - |\hat{A}(Q_l, Q_r)|(Q_r - Q_l)] \quad (4)$$

where $\hat{A}(Q_l, Q_r)$ is the Roe averaged Jacobian matrix. Q_l and Q_r are the state variables to the left and right of the cell interface. The viscous fluxes are central differrenced with second order spatial accuracy. Higher order spatial accuracy is achieved by constructing MUSCL differences through one sided evaluation of Q_l and Q_r with a differentiable limiter such that the solution remains monotone. Experiments with other forms of limiters, such as a minmod limiter, etc. produced less satisfactory results. On the left hand side of Eq.(2), the original ADI operator of the Beam-Warming method is written using diagonal form and the flux vector splitting technique. The left hand side consists of three lower (L), diagonal(D) and upper(U) operators that require three sweeps for each direction.

Grid Generation and Boundary Conditions

An algebraic grid generation scheme based on generalized interpolation scheme was used in generating the grids for the various 2-D and 3-D problems. The grids constructed were nearly orthogonal to the wall boundaries. Numerical solutions were obtained with three different grids (coarse, medium and fine) for most problems. In few cases solutions were obtained only with two grids. The two-dimesional ramp flows were set up as three-dimensional problem by constructing three planes parallel to one another. the two-dimensionality of the flow was enforced through boundary conditions on the two outer planes.

All the boundary conditions were applied in an explicit manner. If the boundary point was a supersonic inflow point, then inflow conditions were specified. At the outflow points simple extrapolation of the flow variables were used to obtain the boundary values. The grids used in all the cases were selected such that the outer boundary points were either in the freestream or on the outflow. At the wall, noslip and specified wall temperatures or adiabatic wall boundary conditions were applied. At the plane of symmetry or at the side boundaries appropriate boundary conditions (symmetry, inflow or outflow) were applied.

Numerical Results

Flow over 2-D Ramp : Problems 3.1 - 3.6

Solutions to problem 3.1, 3.2, 3.4, 3.5 and 3.6 were obtained on three different (51x31, 51x51, 101x81) grids and only the fine grid solutions are presented here. The grid points were clustered close to the leading edge for problem 3.1 and 3.4. For all other problems, the clustering was done at the corner region. In Figure 1. heat transfer coefficient along the wall is shown. The pressure and skin friction coefficients were smooth and the profiles were similar to the heat transfer coefficient and they are not shown here. The solutions differed very little between the medium and fine grids. For problem 3.2, the skin friction coefficient along the wall is shown in Figure 2 and heat transfer coefficient in Figure 3. Only the fine grid results are presented here. As the grids were modified and refined, the size of the separation buble increased and no asymptotic value could be obtained from these computations.

Skin friction and heat transfer coefficients along the wall are shown in Figure 4 and 5 for problem 3.4. The solutions was very similar to the solution of problem 3.1. In Figures 6 and 7 skin friction and heat transfer coefficients for Problem 3.5 are presented. Solution dependency on grids were explored with three different grids and the computed solutions with the three grids did not show any convergence to an unique state. The size of the separation buble grew with grid refinement. The same observation can also be made for problems 3.2 and 3.6. The skin friction coefficients for problem 3.5, from the three different grids, are shown in Figure 8. The 51x51 grid predicts the separation buble size consistant with experimental observations but computations with the finer grid showed the separation point to move upstream and the reattachment point to move downstream. Further refinement and adaptive grid studies are underway to resolve this issue. At this time it is not clear why the solutions did not converge to an unique state. In Figures 9 and 10 skin friction and heat transfer coefficints for problem 3.6 are shown. Numerical solutions to problems 3.2, 3.5 and 3.6 showed a primary and a small secondary separation zone. The small secondary separation buble was observed only with the finer grids in these cases.

Flow over 3-D Obstacle : Problems 4.1 and 4.2

Two different grids (51x51x19 and 51x81x19) were used for both problems 4.1 and 4.2 and only the fine grid solutions are presented here. The size of the separation buble did not increase significantly with the finer grid. Computed presure, skin friction and heat transfer coefficients along the wall at three diffrent cross sections (sections A, C and D

) are shown in Figures 11, 12 and 13 for problem 4.1 and in Figures 16, 17 and 18 for problem 4.2 respectively. The skin friction lines on the wall projected on to the z=0 plane are shown in Figures 14 and 19 for problems 4.1 and 4.2 respectively. Only one half (y $>$ 0) of the geometry is shown in these figures. By making use of symmetry the other half of the physical domain was elliminated from the the computational domain. Iso-Mach lines on the symmetry plane (y = 0) are shown in Figures 15, for problem 4.1 and in Figure 20 for problem 4.2. The computational results show significant difference in flow characteristics between problem 4.1 and 4.2. Only one separation buble was observed for problem 4.1 whereas a secondary recirculation zone was observed for problem 4.2 and is evident in Figure 19. The presence of the secondary separtion buble is also evident in the skin friction and heat transfer coefficints shown in Figure 17 and 18. The orientation of the primary separation line to the free stream direction differ significantly between the two cases. For problem 4.1 the primary separation line is oriented with the sweep line, whereas for problem 4.2, the separation line is divergent with the sweep line and propagates upstream away from the symmetry plane.

Computer Resource Requirements

The Cray YMP at NASA Ames was used for all the above computations. Between 3 and 4 orders of magnituide change in L2 norm of the change in conservative variables was obtained in approximately 2000 steps for most case. The code required 0.00001 CPU seconds per iteration per grid point and 1.0 MW of CRAY YMP memory was required for 25,000 grid points.

References

[1] Obayashi, S. ,"Numerical Simulation of Underexpanded Plumes using Upwind Algorithms," AIAA Paper 88-4360-CP, 1988.

[2] Venkatapathy, E., Feiereisen, W. J. and Obayashi, S., ,"Computational Studies of Hard Body and 3-D Effects in Plume Flows," AIAA Paper 88-3158, 1988.

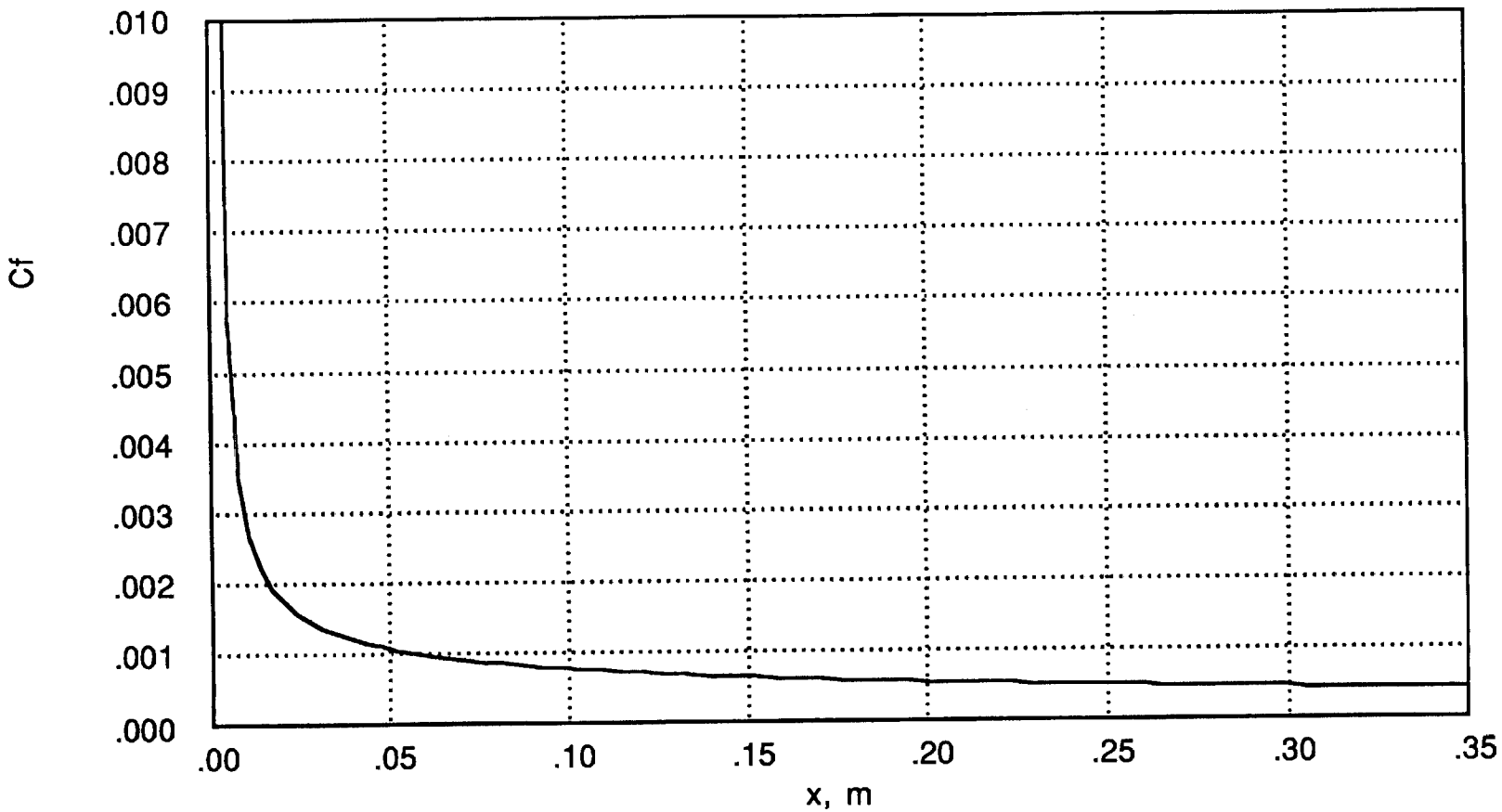

FIGURE 1. CASE 3.1 - SKIN FRICTION COEFFICIENT C_f ALONG THE WALL

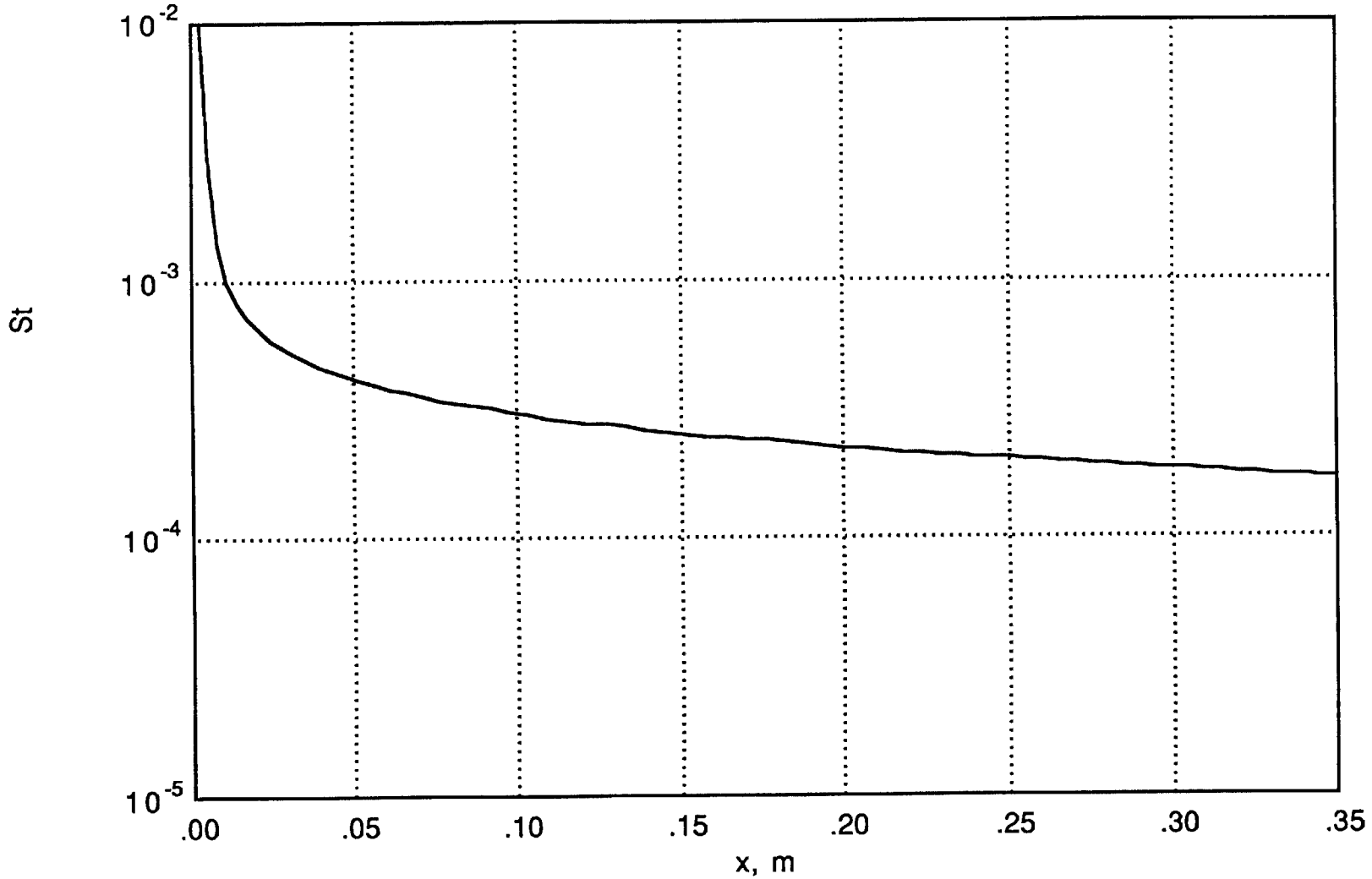

FIGURE 1. CASE 3.1 - HEAT TRANSFER COEFFICIENT S_t ALONG THE WALL

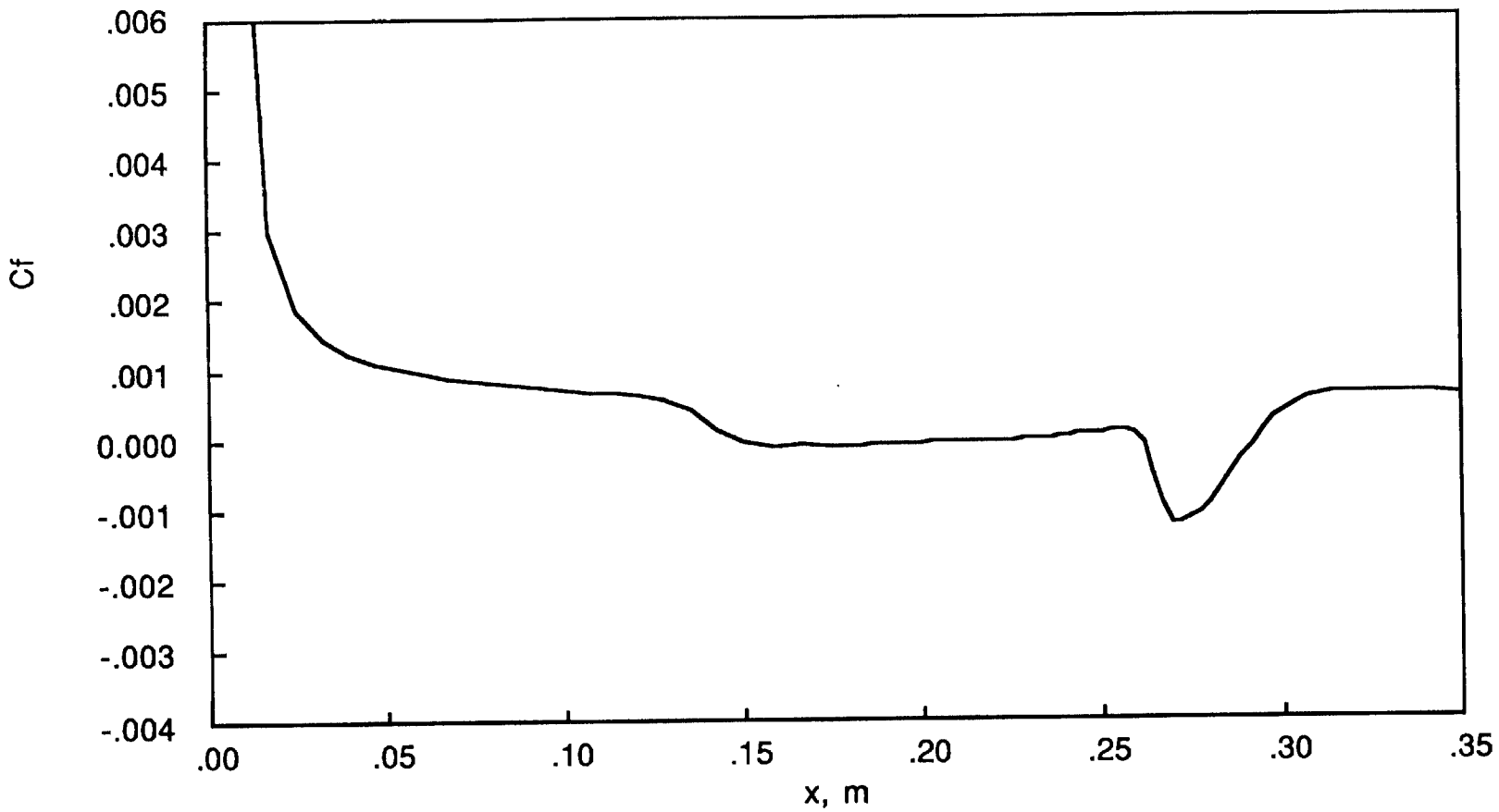

FIGURE 2. CASE 3.2 - SKIN FRICTION COEFFICIENT C_f ALONG THE WALL

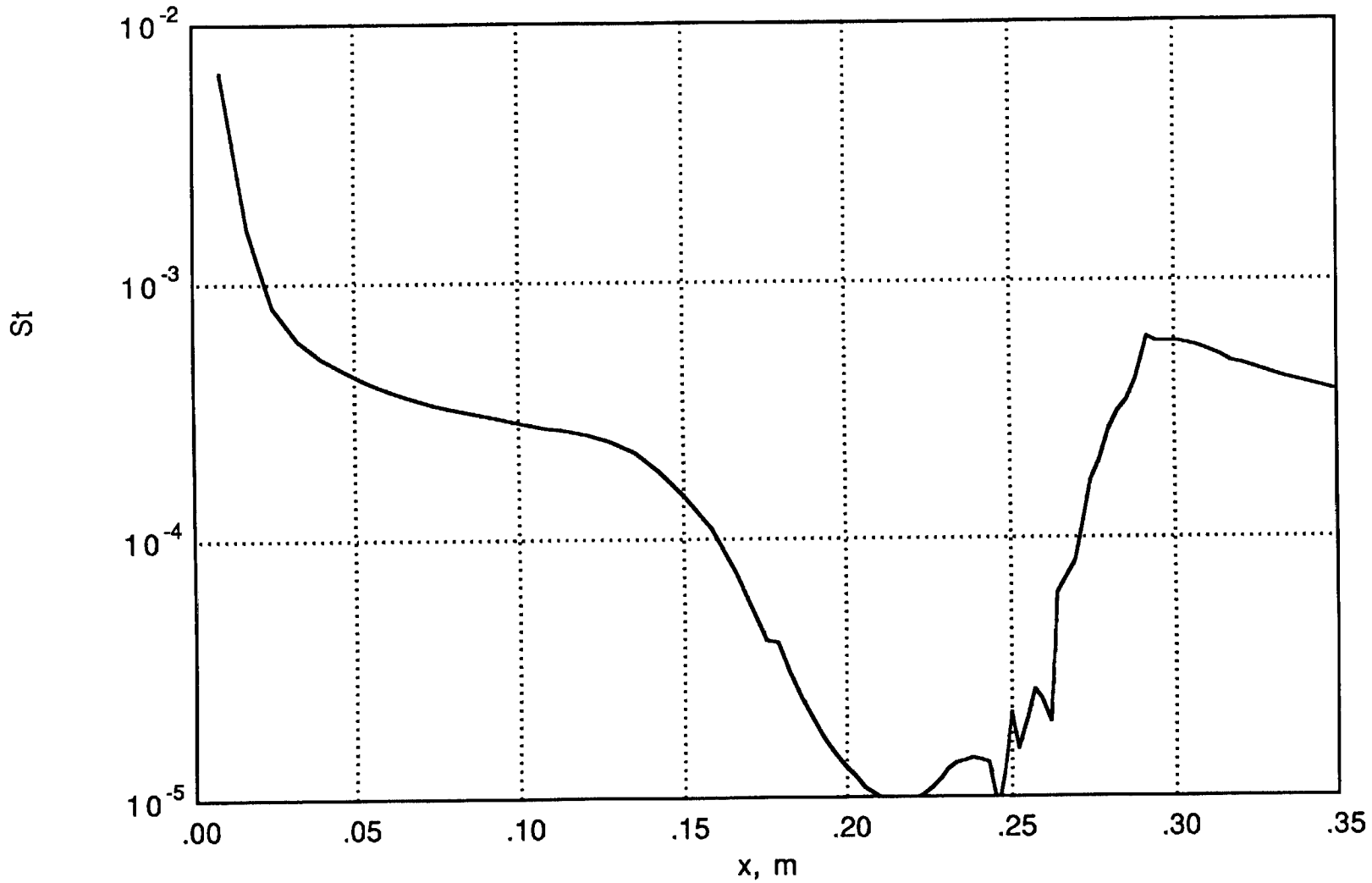

FIGURE 3. CASE 3.2 - HEAT TRANSFER COEFFICIENT S_t ALONG THE WALL

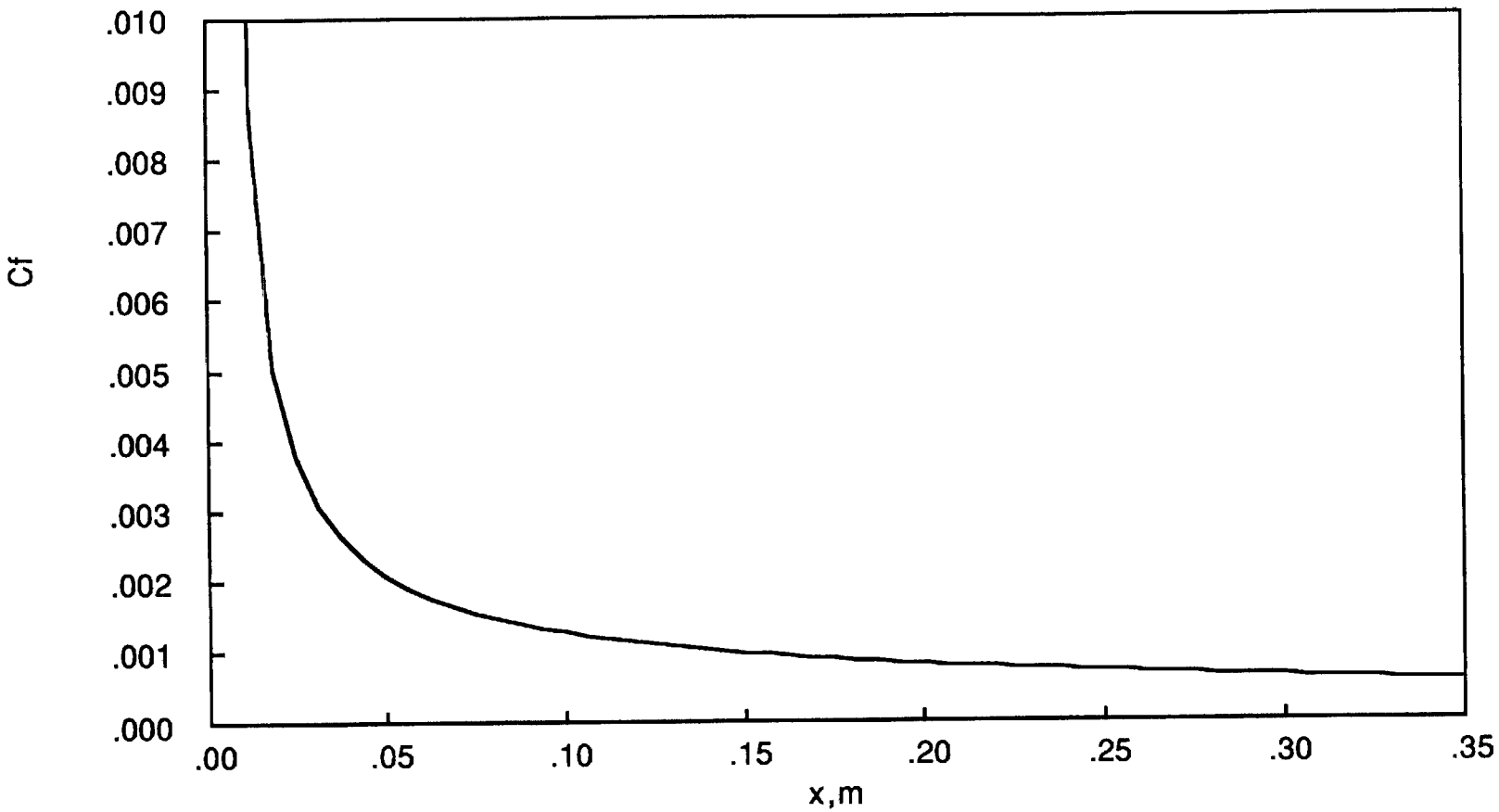

FIGURE 4. CASE 3.4 - SKIN FRICTION COEFFICIENT C_f ALONG THE WALL

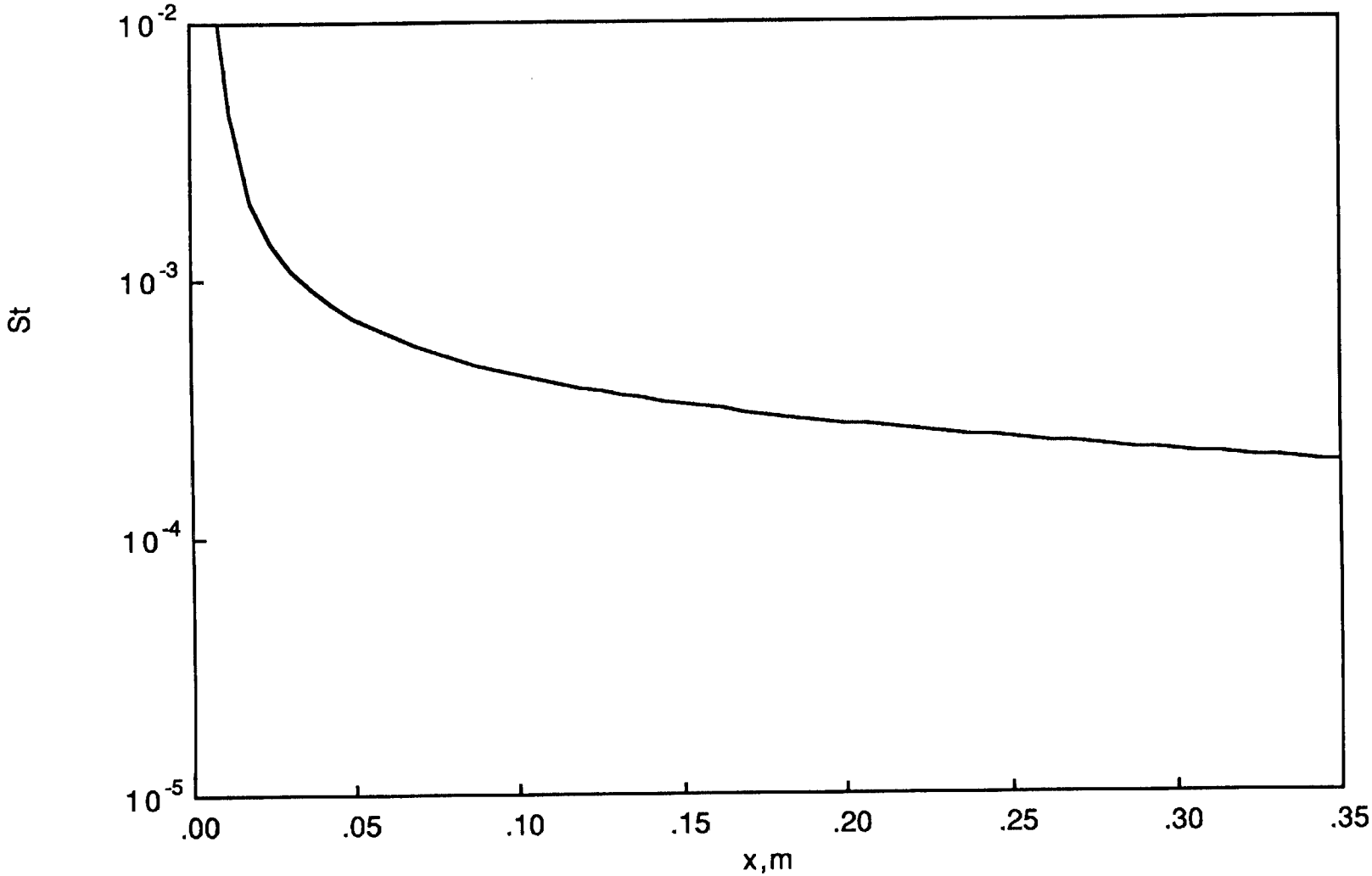

FIGURE 5. CASE 3.4 - HEAT TRANSFER COEFFICIENT S_t ALONG THE WALL

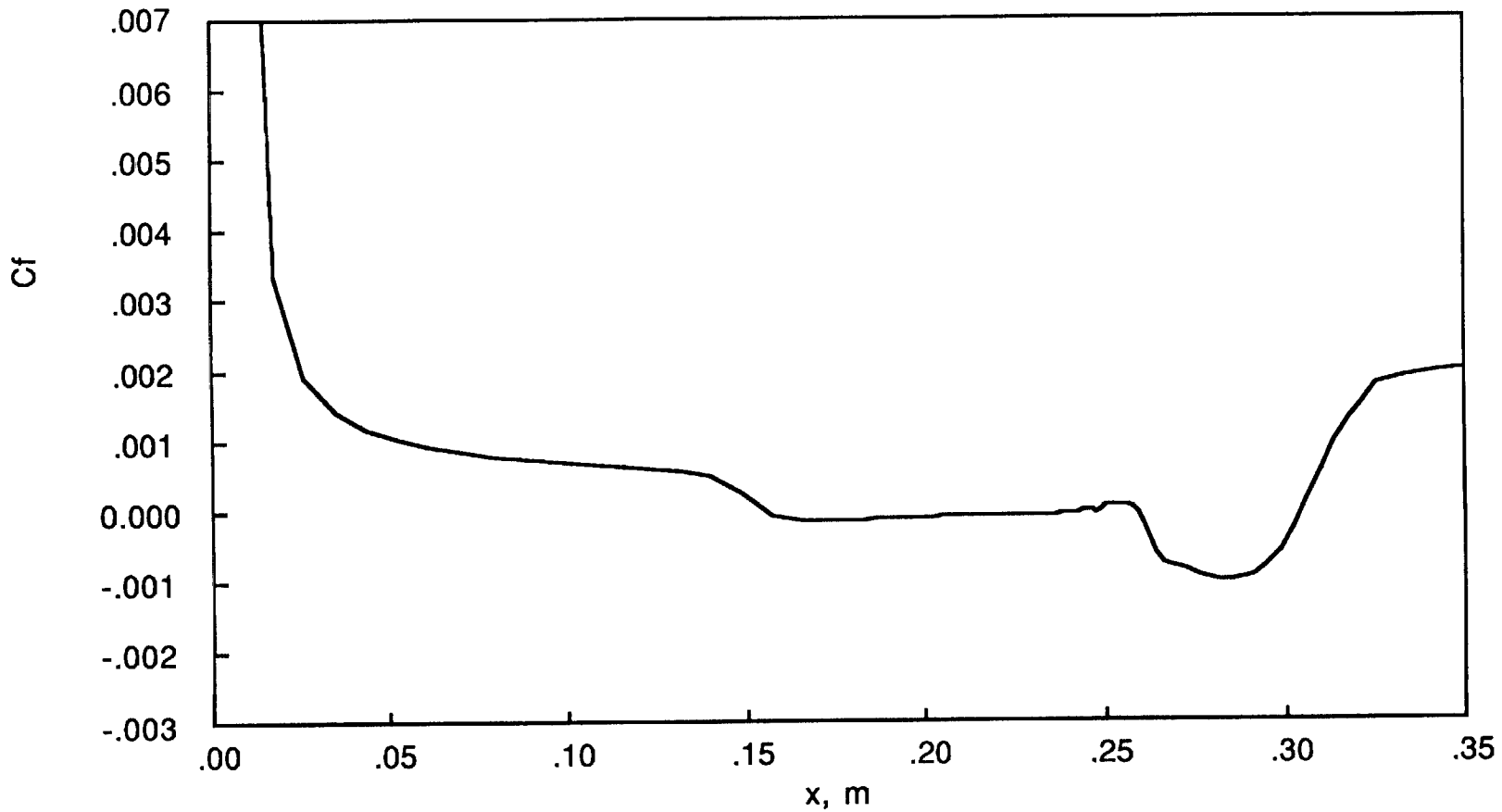

FIGURE 6. CASE 3.5 - SKIN FRICTION COEFFICIENT C_f ALONG THE WALL

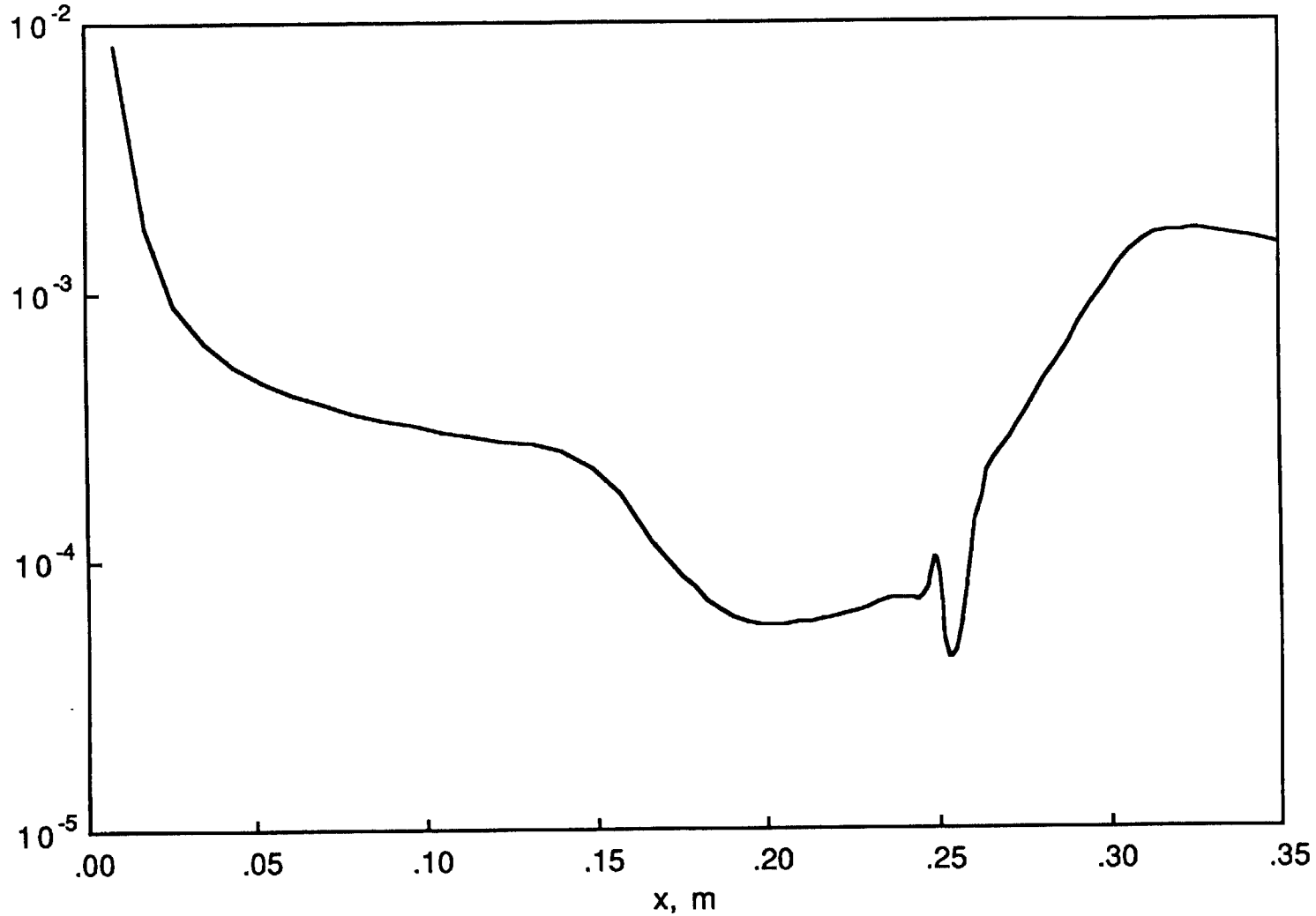

FIGURE 7. CASE 3.5 - HEAT TRANSFER COEFFICIENT S_t ALONG THE WALL

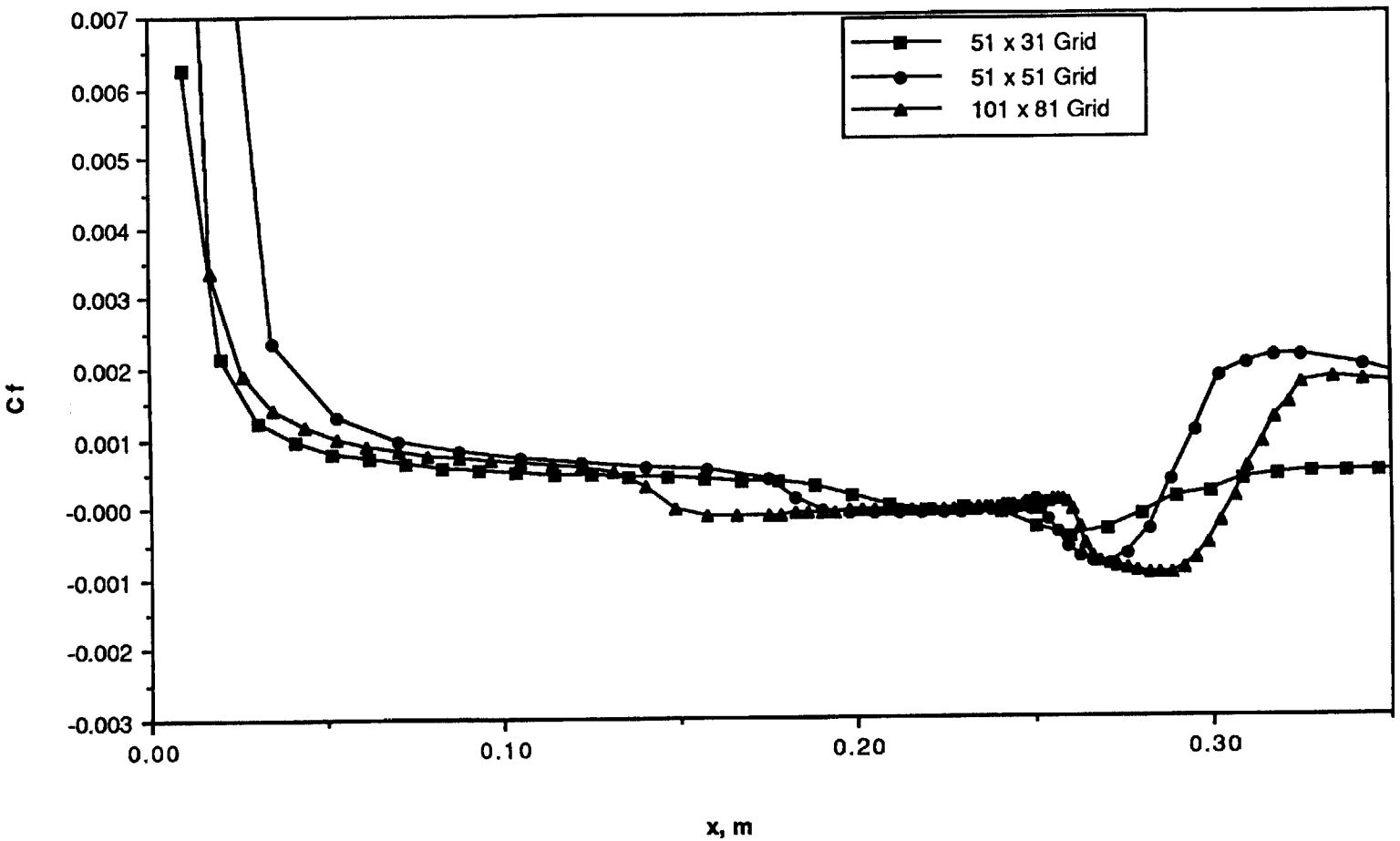

FIGURE 8. WALL SKIN FRICTION C_f, COMPARISON ON 3 GRIDS - CASE 3.5

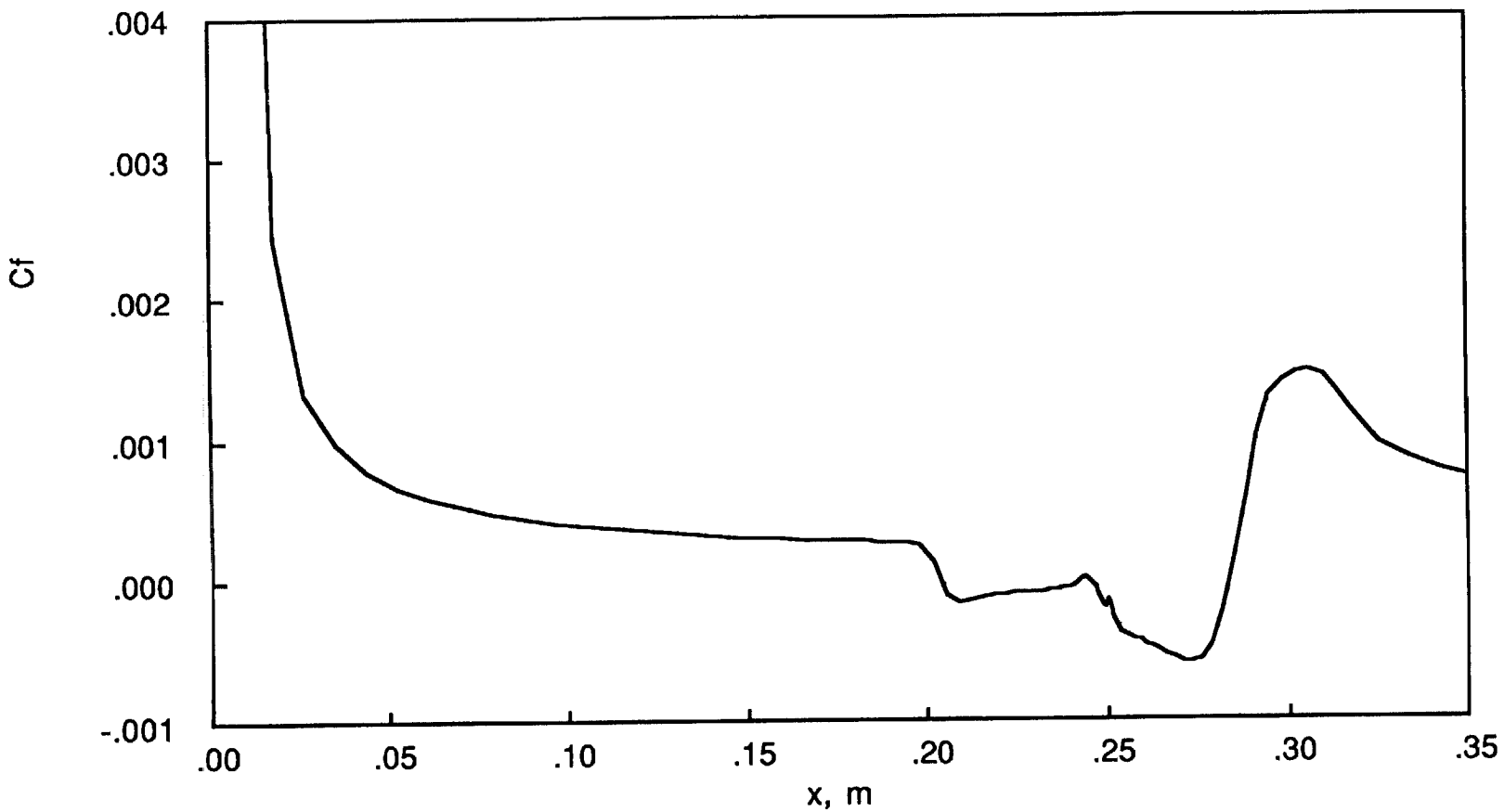

FIGURE 9. CASE 3.6 - SKIN FRICTION COEFFICIENT C_f ALONG THE WALL

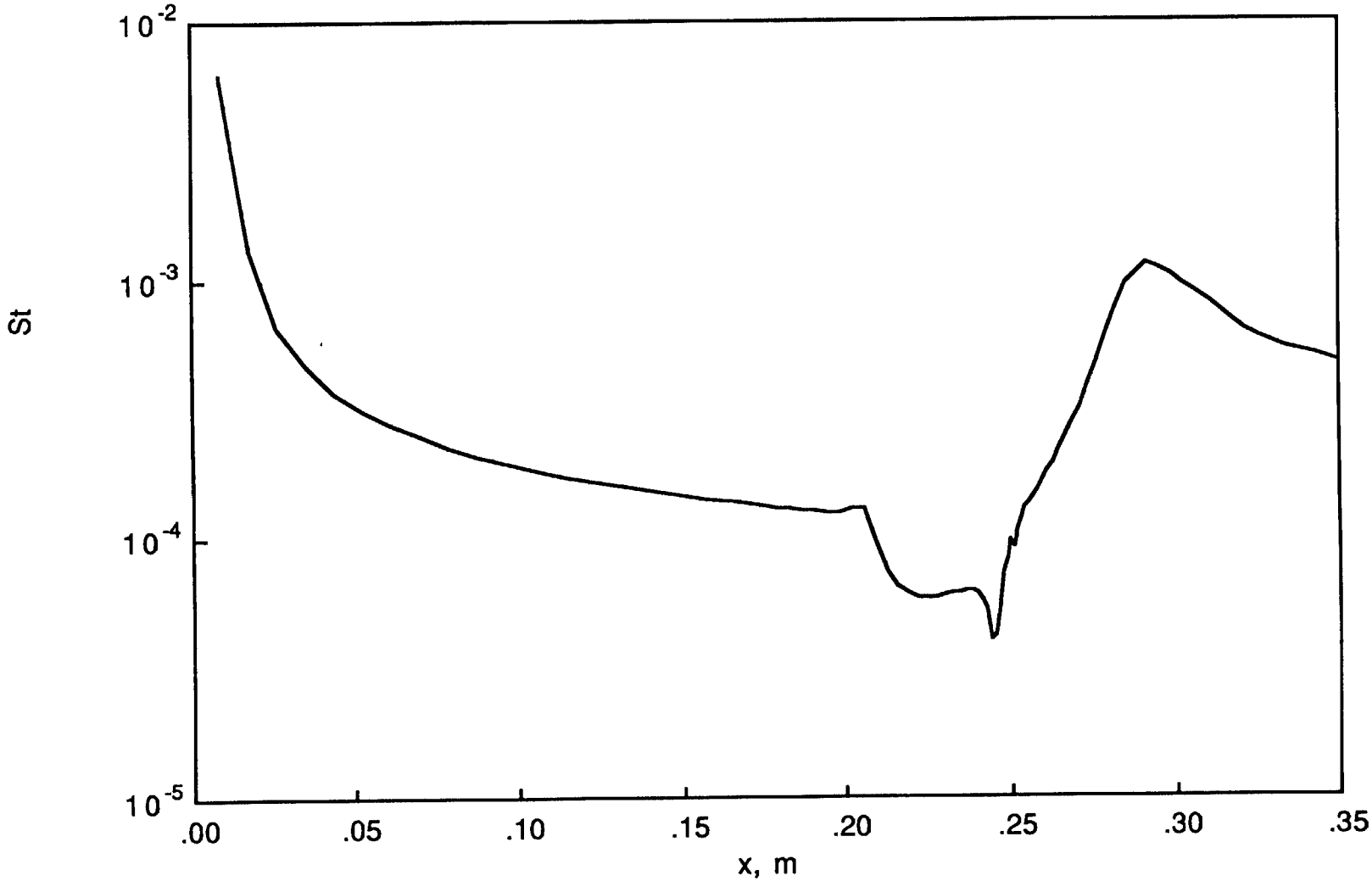

FIGURE 10. CASE 3.6 - HEAT TRANSFER COEFFICIENT S_t ALONG THE WALL

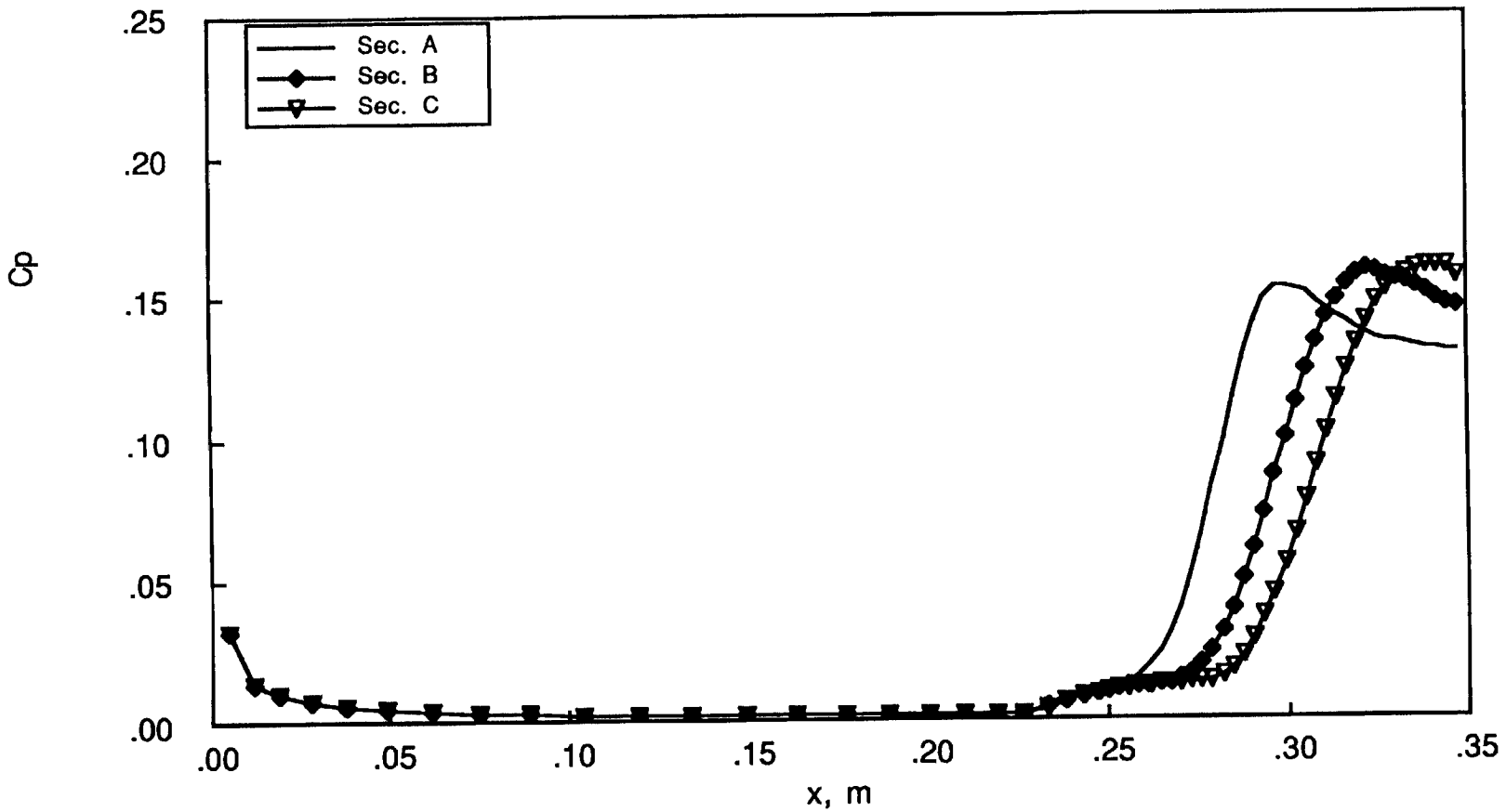

FIGURE 11. CASE 4.1 - PRESSURE COEFFICIENT C_p ALONG THE WALL

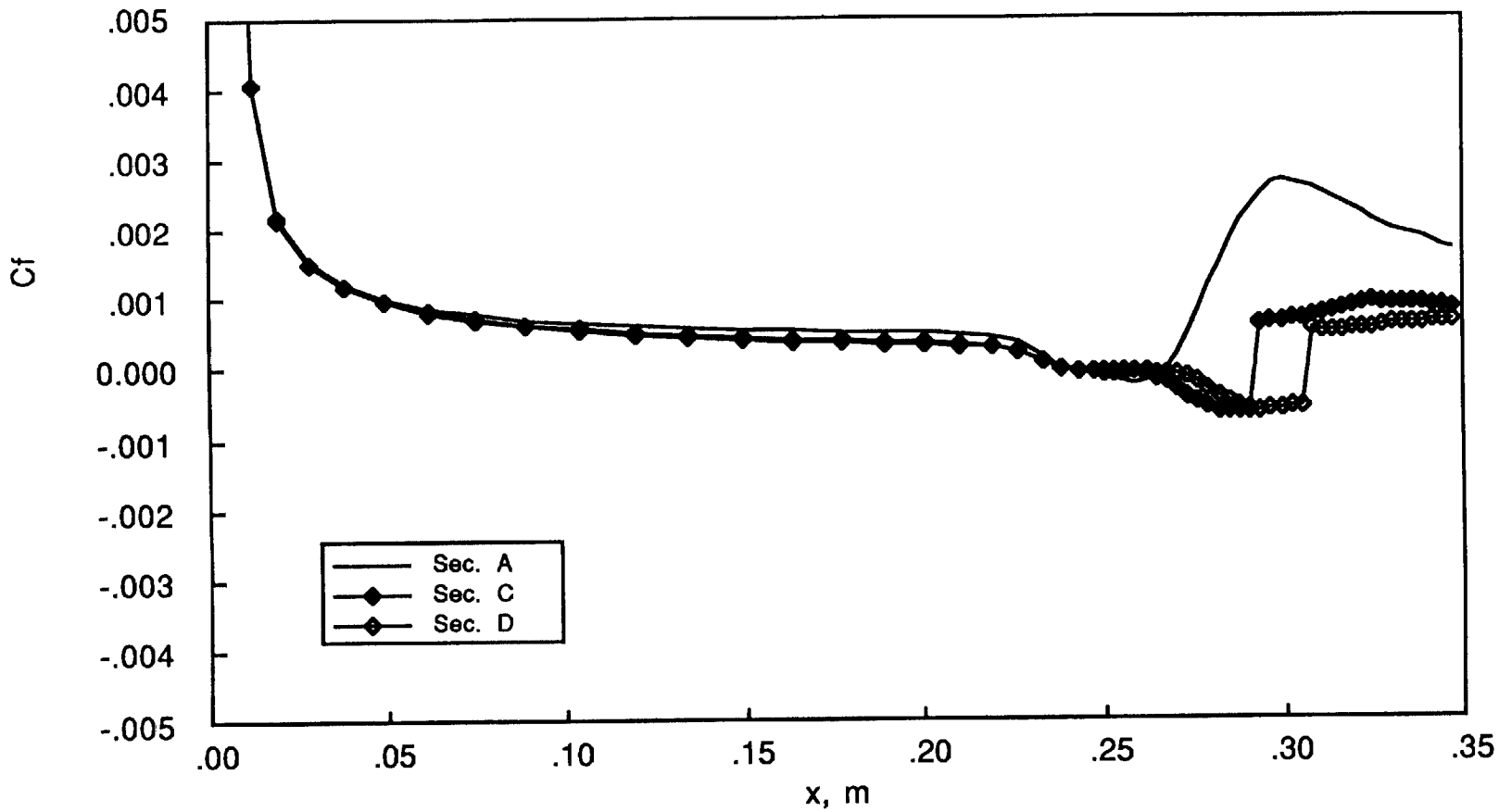

FIGURE 12. CASE 4.1 - SKIN FRICTION COEFFICIENT C_f ALONG THE WALL

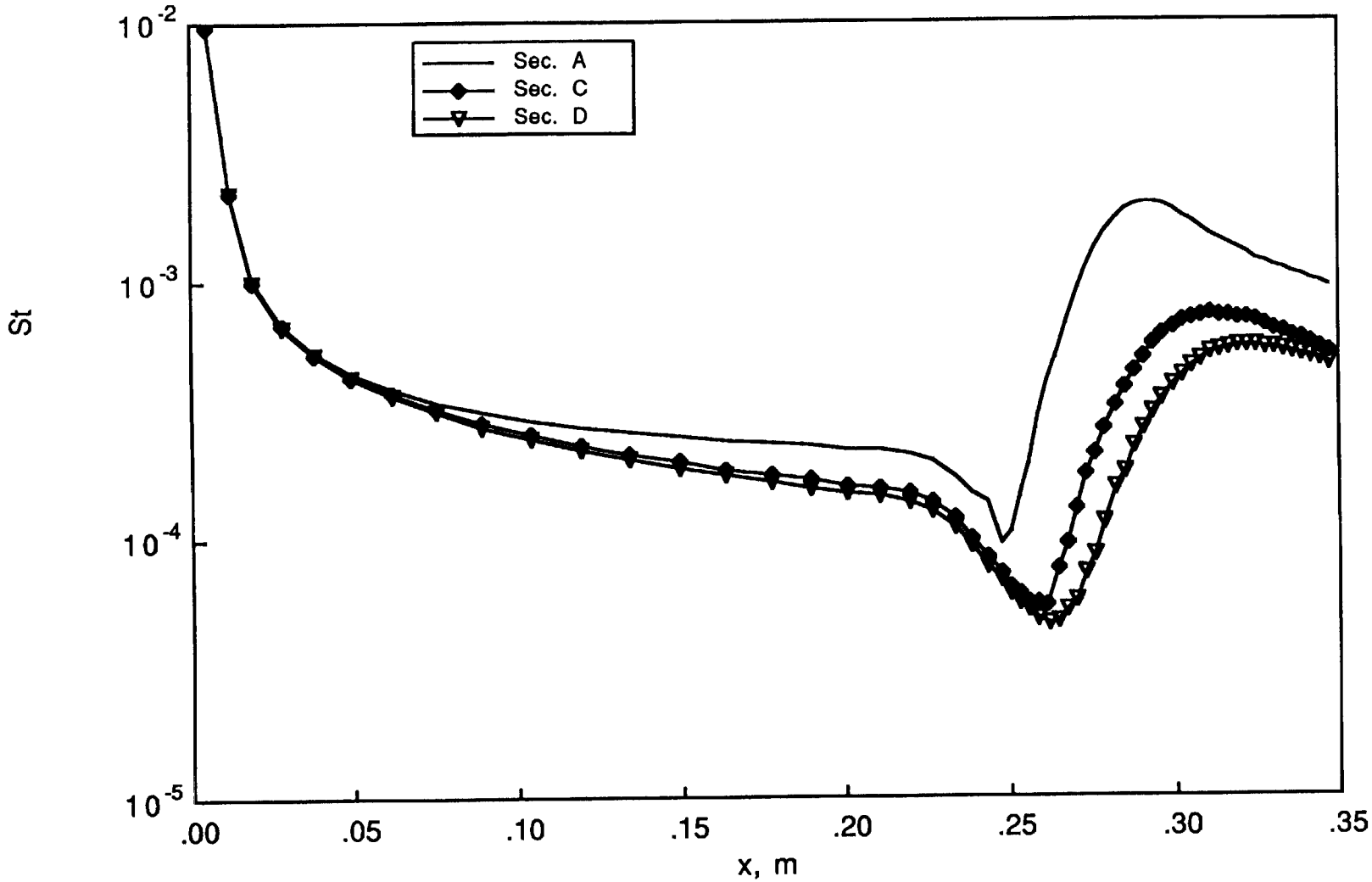

FIGURE 13. CASE 4.1 - HEAT TRANSFER COEFFICIENT S_t ALONG THE WALL

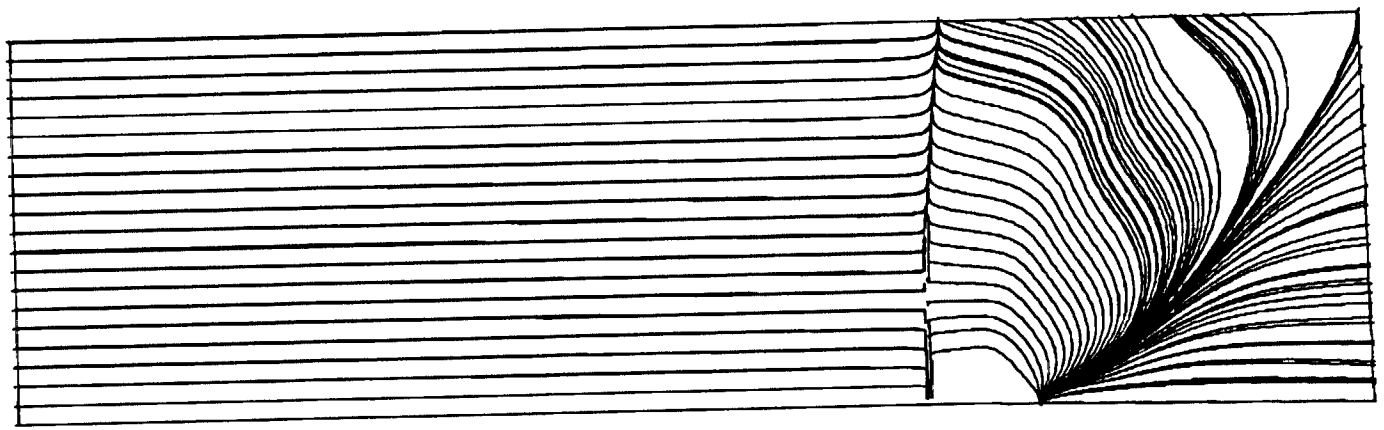

FIGURE 14. CASE 4.1 - SKIN FRICTION LINES (OIL FLOW PATTERN) ON Z = 0 PLNAE

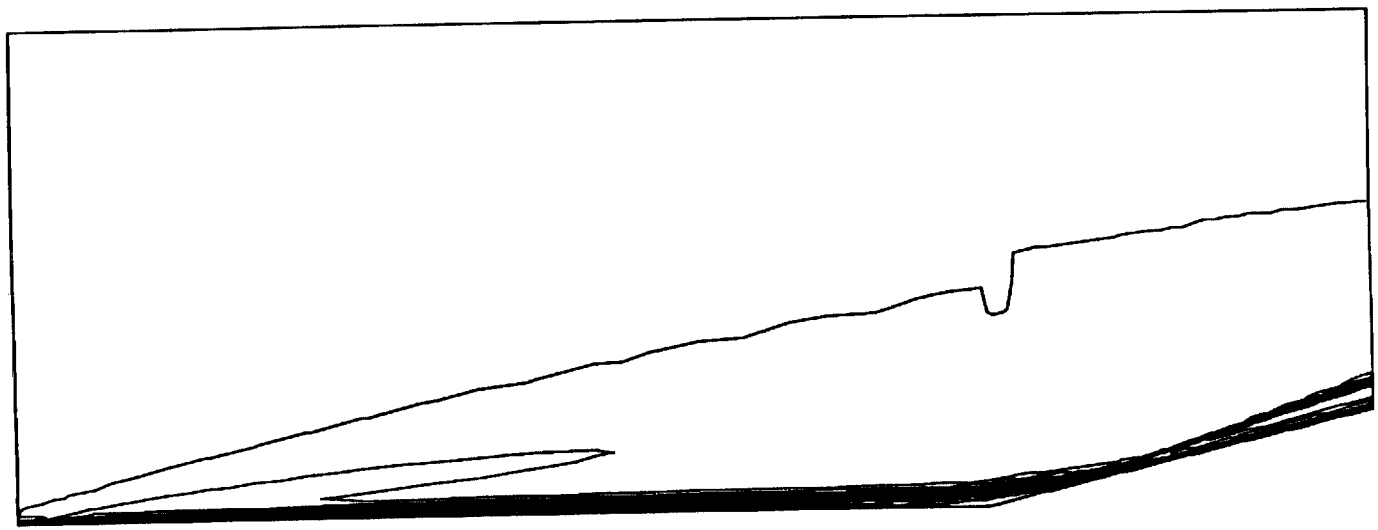

FIGURE 15. CASE 4.1 - ISO-MACH LINES ON (Y=0) SYMMETRY PLANE

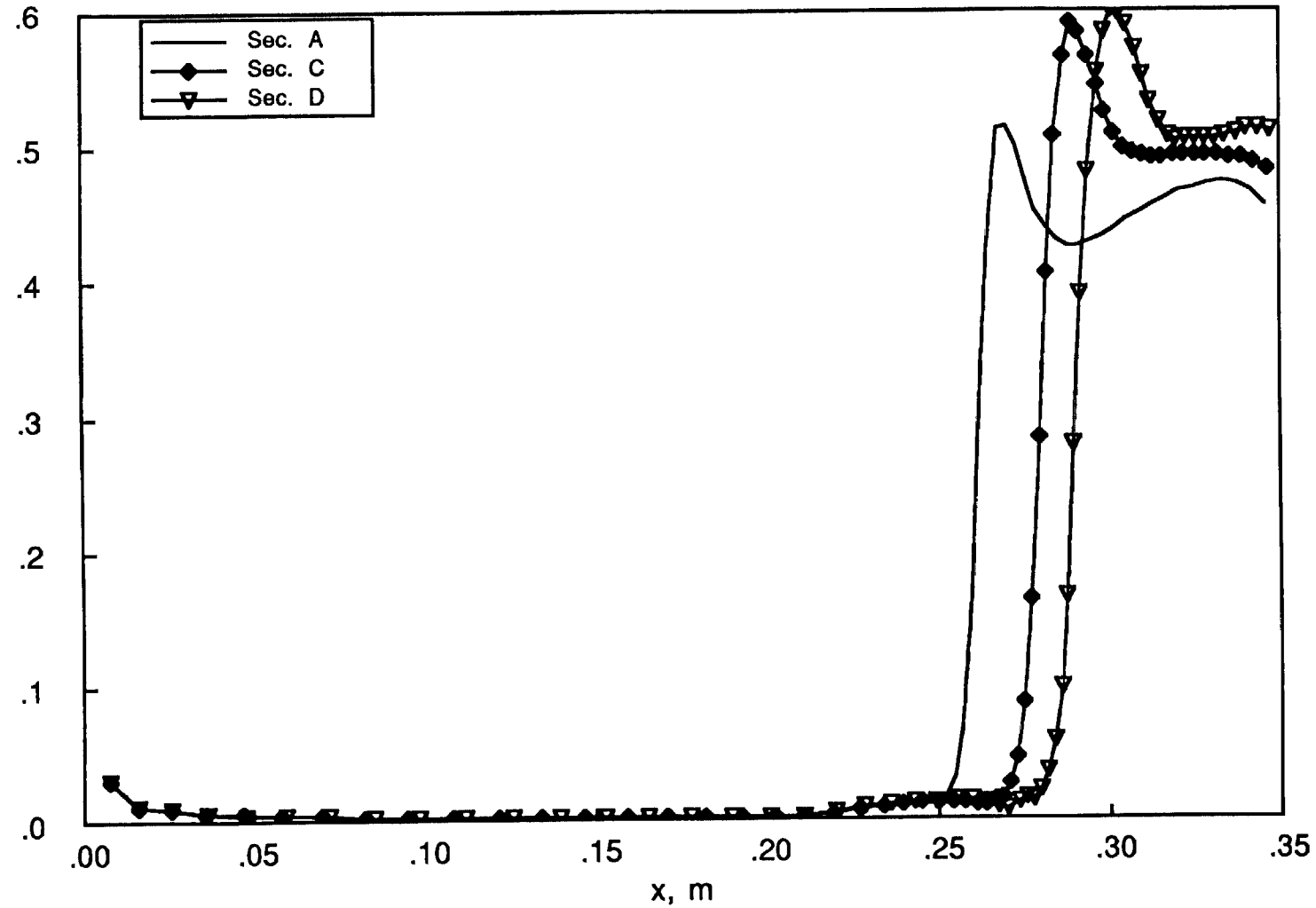

FIGURE 16. CASE 4.2 - PRESSURE COEFFICIENT C_p ALONG THE WALL

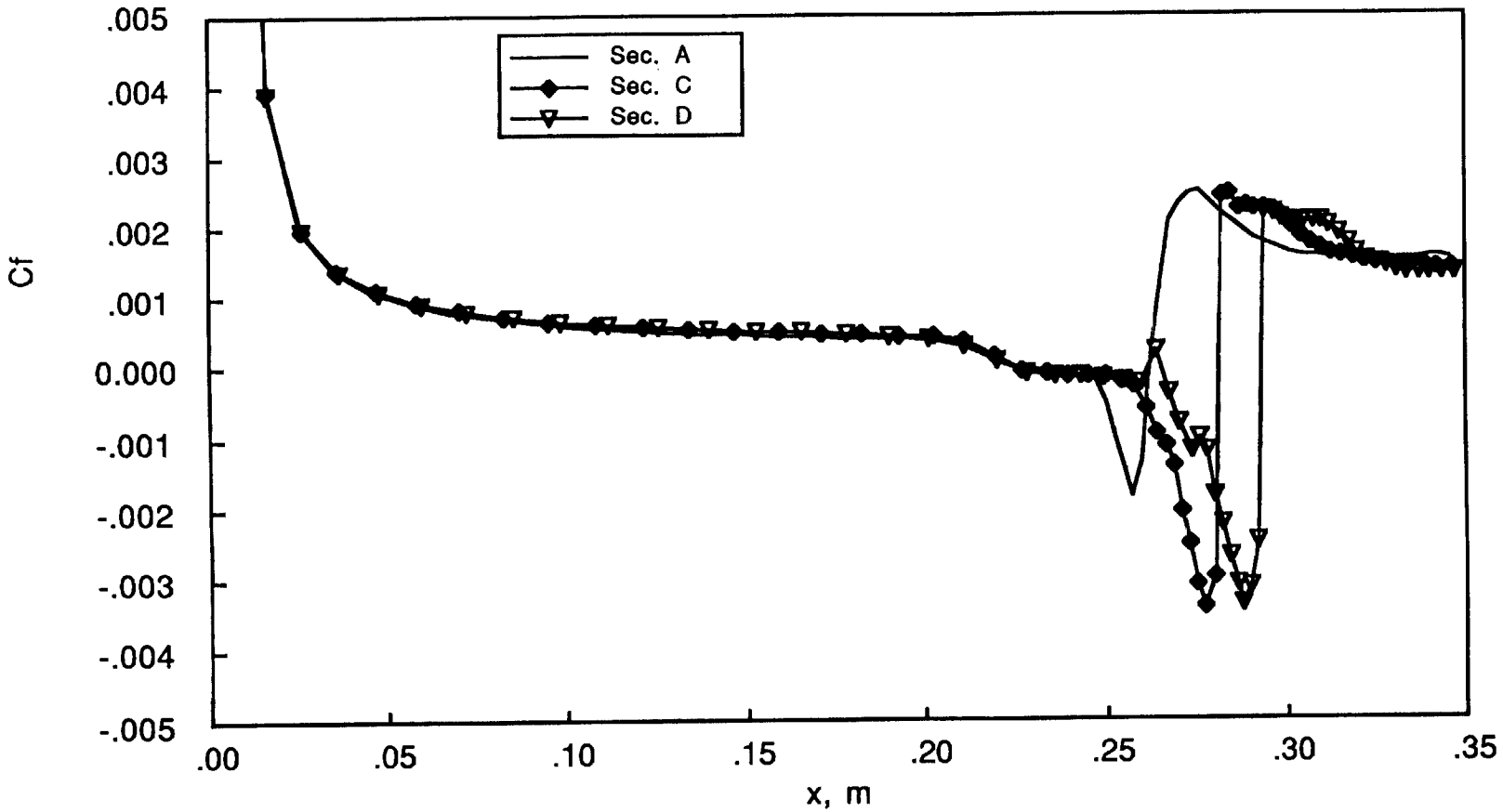

FIGURE 17. CASE 4.2 - SKIN FRICTION COEFFICIENT C_f ALONG THE WALL

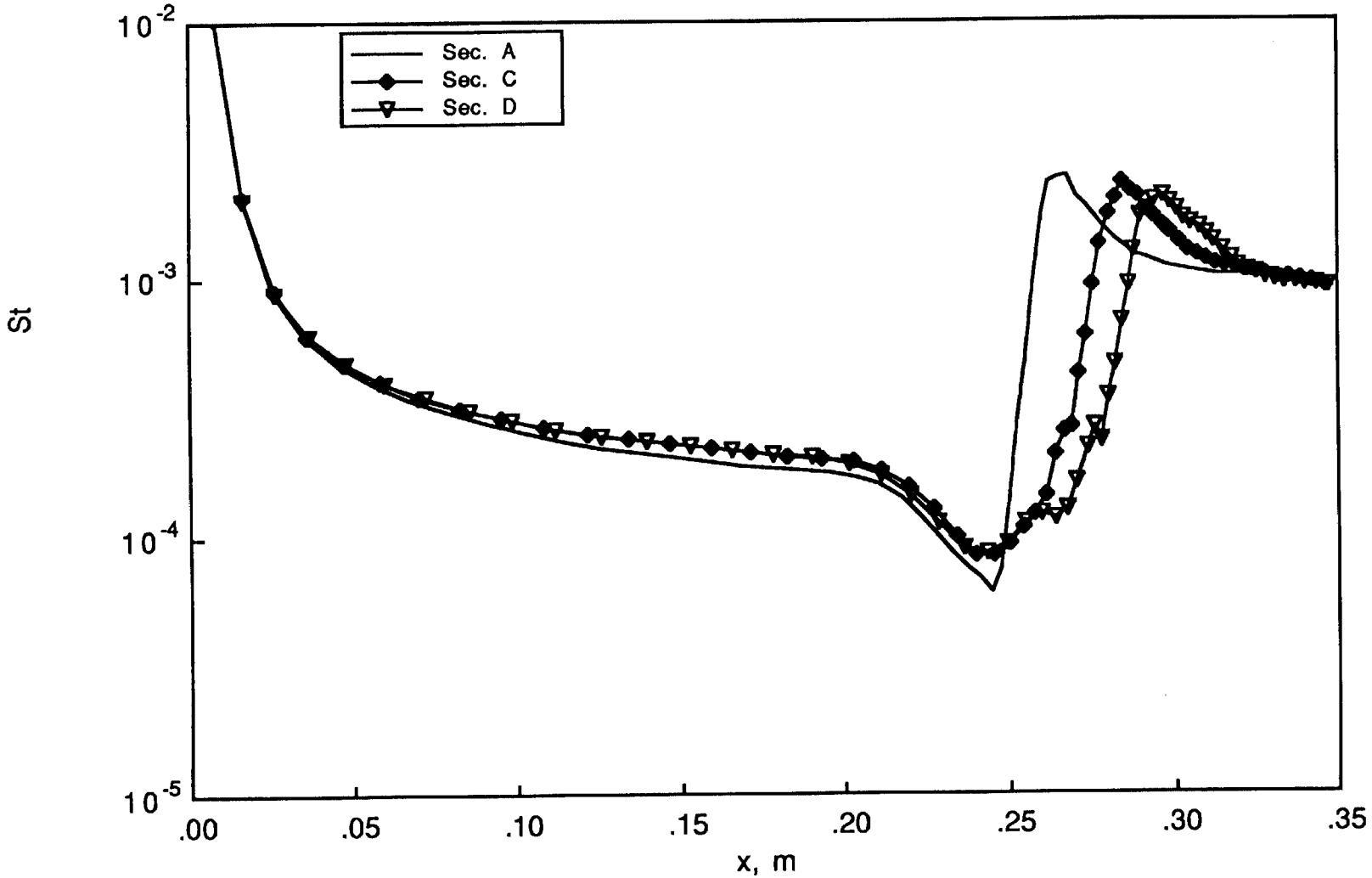

FIGURE 18. CASE 4.2 - HEAT TRANSFER COEFFICIENT S_t ALONG THE WALL

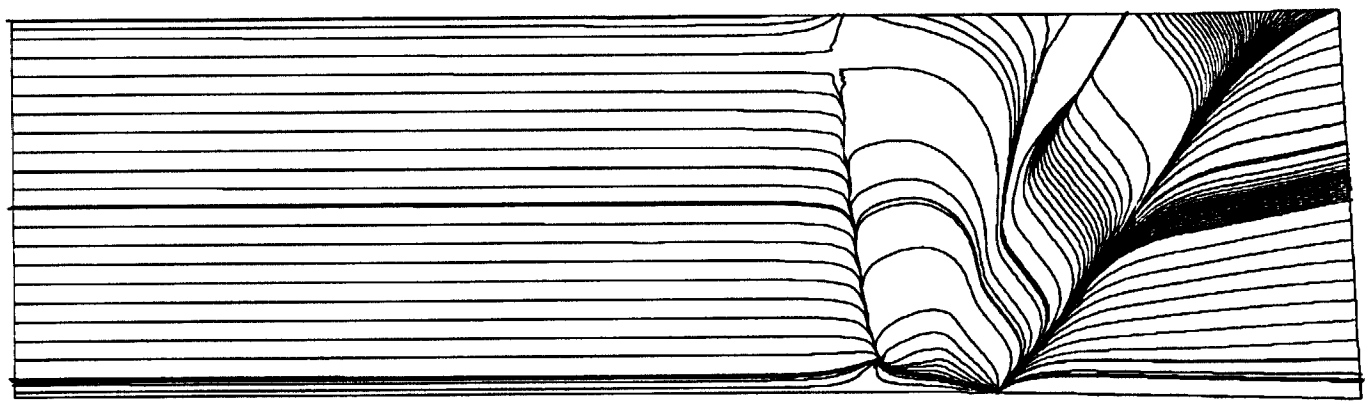

FIGURE 19. CASE 4.2 - SKIN FRICTION LINES (OIL FLOW PATTERN) ON Z = 0 PLNAE

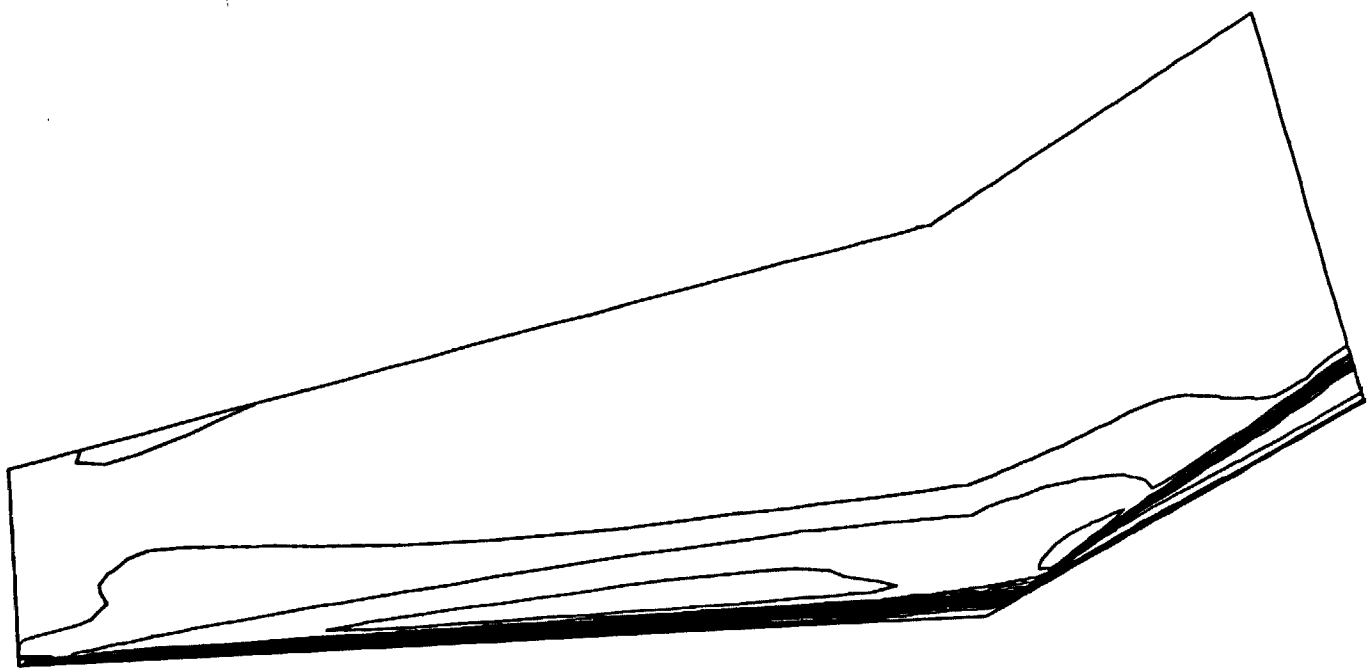

FIGURE 20. CASE 4.2 - ISO-MACH LINES ON (Y=0) SYMMETRY PLANE